Hyperspectral Oblique Plane Microscopy - Methods and Supplementary Information

Ke Guo, Konstantinos Kalyviotis, Periklis Pantazis, Christopher J Rowlands

1 Methods

1.1 Instrument construction

For reasons of user familiarity and ease of use, λ-OPM was constructed as an add-on to a commercial microscope frame (Olympus IX73). A laser beam (Coherent Obis 488nm LX 150mW, or LaserQuantum Gem 660nm 1W) is focused (through part of the imaging path) to a spot near the edge of the back focal plane of a water immersion objective (O1, 25× NA=1.1, Nikon MRD77220 mounted in a custom nosepiece), producing a weakly-focused thin line in the sample, tilted at an angle of 38°. Scattered or fluorescent light from the line is collected by the same objective, and ultimately imaged onto the remote focusing plane, with an overall magnification of approximately 1.33×. This overall magnification must be equal to the refractive index of the sample, in accordance with the remote focusing principle [1]. Matching the refractive index is achieved by splitting the penultimate lens into two physical lenses (Thor Labs TTL200MP and AC508-750-A-ML), and tuning their separation to change their effective overall focal length (and thus the magnification of the system). The light then passes into O2 (air immersion, 20× NA=0.7, Olympus UCPLFLN20X) to form a theoretically-perfect remotely-focussed image. The back aperture of O2 is slight smaller than the image of the back aperture of O1 and a misalignment between them can reduce the resolution and introduce aberrations. Therefore, O2 is mounted on a three-axis translation stage (Newport M-561D-XYZ with two SM-13 micrometers for XY positioning and a DS-4F differential micrometer for Z focusing) for fine position adjustment.

The remote focusing plane lies on the outer surface of a coverslip, which functions as a wall of a custom-made water chamber (see Section 3.1). The image is refracted through the coverslip and water into a third objective (O3, 25× NA=1.1, Nikon MRD77220) with the front mounted inside the water chamber. The optical axis of O3 is tilted by 38° so that the remote plane is normal to its optical axis and a translation mount is used on O2 to match the field of view of O2 and O3. The refraction by the water chamber negates the NA loss due to the mismatch of the light cones of O2 and O3 caused by the tilt [2]. The line illuminated by the laser is finally imaged horizontally (in the x direction) on to a camera with a total magnification of 33×. For the spectral resolution, a horizontal grating (ThorLabs GR25-0310, 300 lp/mm, 8.4 ° blaze angle, tilted by approximately 5 °) is inserted using a custom insert (see Supplementary section 3.2) in a commercial kinematic fluorescence filter cube (ThorLabs DFM1/M) between O3 and the tube lens before a second camera. This grating diffracts (first order) the image in the y direction as a function of wavelength, creating a hyperspectral image with as many as 2560 spectra captured simultaneously (i.e. one spectrum per column in the image).

λ-OPM can be used to measure both fluorescence and Raman spectra over different spectral ranges with different beamsplitter and filter sets which can be easily inserted between Galvo y and O2 using commercial kinematic fluorescence filter cubes (ThorLabs DFM1/M). The fluorescence measurements were conducted using the 488 nm laser, and a dichroic beamsplitter and a bandpass filter (Semrock FF497-Di01 and FF01-565/133-25) were used. For Raman scattering measurements, the beamsplitter and filter set was replaced by a different dichroic beamsplitter and a longpass filter (Semrock Di03-R660 and LP02-664RU respectively). Furthermore, an extra longpass filter (Semrock LP02-664RU) was added in front of the grating to filter out any stray laser light that reaches O3.

1.2 Sample preparation

1.2.1 Fluorescent emulsion

Four different aqueous solutions of quantum dots (CdSeS/ZnS alloyed 525 nm, 575 nm, and 630 nm, CdSe/ZnS core-shell 600 nm from Sigma-Aldrich) were diluted by 10 %. The 550 nm quantum dots solution was prepared by mixing water with CdTe quantum dot powder (PlasmaChem). The organic solution is prepared by mixing engineering fluid HFE 7500, fluosurf solution (5 % in HFE 7500), and hexane with a ratio of 1:1:5.4 to reach a refractive index close to water. The quantum dots solutions, 50 µL each, were then mixed with more than 40 μL organic solution in separate Eppendorf tubes and shaken to form emulsions with small water bubbles. An M6 nut was glued using UV glue in the confocal dish to work like a well. All emulsions were added into the nut a confocal dish and gently stirred using a pipette tip. Excessive perturbation can result in large bubbles and should be avoided. The sample was then cover by a lid to reduce evaporation of the organic solvents.

1.2.2 Polymer particles in agarose

The PS (6-10 µm from Sigma-Aldrich), PMMA (6-10 µm from Goodfellow), and PA6 (5-50 µm from Goodfellow) particles were pre-mixed in an eppendorf tube with a ratio of about 1:1:1 using a vortex mixer. Approx. 0.004 g of the polymer mix was mixed into 1 mL melted 2 % agarose gel, and immediately dropped into a confocal dish to create a pad. The samples used for CNN training was prepared in the same way by separately adding each polymer particles into 2 % agarose gel with slightly higher concentration.

1.2.3 Zebrafish husbandry

Experiments involving zebrafish were conducted in accordance with UK Home Office requirements (Animals Scientific Procedures Act 1986, project license P219D3ABD). All experiments were conducted up to 5 days post-fertilization (dpf). At 24 hours post fertilisation (hpf), PTU (Merck) was added to the E3 medium in order to reduce pigmentation.

1.2.4 Zebrafish myotome wound experiments

Wild-type (WT/AB) embryos at 3dpf were anaesthetised in 4.2 % w/v MS222 (Merck) and mounted on 1.2 % w/v/ low-melting point agarose (Merck). The embryos were wounded by making a single incision using a pair of forceps (Dumont No. 5) in the dorsal myotome opposite to the anal pore. After wounding, the embryos were transferred to egg medium (E3) to allow for recovery. Prior to

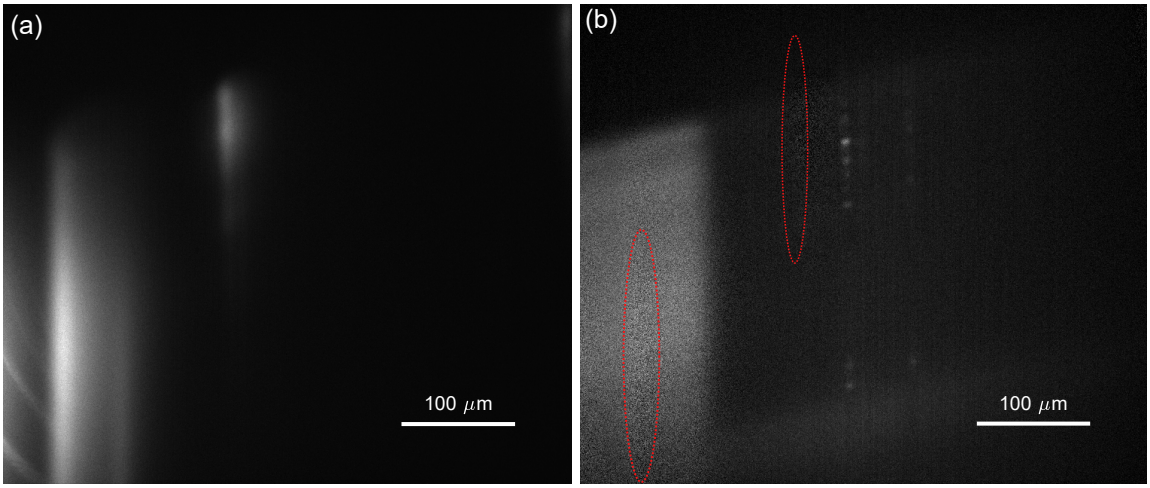

Supplementary Figure 1: (a) An image of the background scattering from intermediate optics. (b) An hyperspsectral image showing artefacts due to errors in background subtraction.

imaging, embryos were anaesthetised and subsequently mounted on 0.7 % w/v low-melting point agarose (Merck) in 20 mm glass-bottom Petri dishes (VWR). A hair loop was used to position the embryos such that the wound was close to the glass surface of the Petri dish. After gelation, each dish was supplemented with 1-2 ml of E3 containing 4.2 % w/v MS222.

2 Alignment and calibration

The optics near the intermediate image plane introduced some strong fluorescence and scattering spots in the hyperspectral image frame. While these could be eliminated by subtracting a blank image, imprecise subtraction (due to sample effects and laser fluctuations) resulted in artefacts as shown in Supplementary Figure. 1, or spurious intensity fluctuation at the corresponding x position in the final map, e.g. in Figure 4(a).

2.1 Spectral calibration

In a hyperspectral image, the horizontal position corresponds to the position along the imaged line, while the vertical position, under the paraxial approximation, is a linear function of the wavelength and the setting of Galvo y, i.e. the vertical position of the imaged line. We used the transmission spectrum of a quad-band bandpass filter (Semrock FF01-446/523/600/677-25) to determine the parameters for spectral calibration. The 488nm laser was spatially filtered, introduced to the OPM using the reflection of a dichoic beamsplitter (Semrock Di01-R405/488/561/635) and was focused to an approximately 0.5 mm spot near the edge of the back focal plane of O1. This results in a line with FWHM 8 to 24 μm across 500 μm through the sample, which in this case was a drop of an aqueous solution of fluorescein. The fluorescence was filtered by the quad-band bandpass filter and imaged in the centre of the camera as shown in Supplementary Figure 2(a). When the grating was introduced, the image broadened in the y direction showing two bright transmission bands as

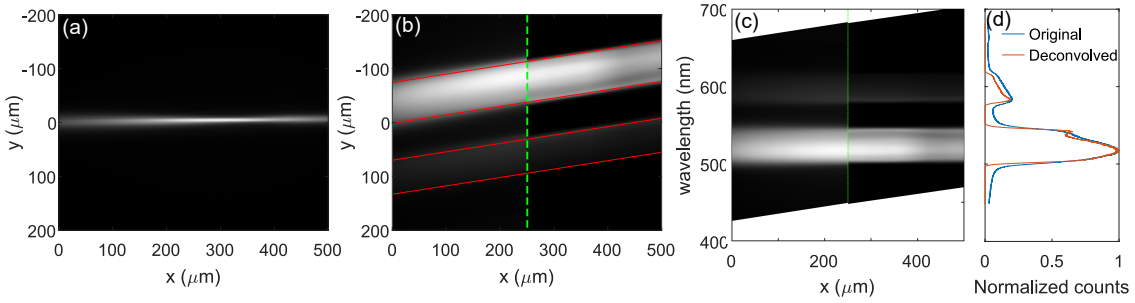

Supplementary Figure 2: (a) An example image of a fluorescent line from an aqueous solution of fluorescein (11 wt%). (b) An example of a hyperspectral image from the same sample, filtered using a quad-band bandpass filter (Semrock FF01-446/523/600/677-25). The red lines correspond to 4 band edges of the filter: 502.5 nm, 544.5 nm, 582.5 nm and 617.5 nm. The right side of the image is sharpened by deconvolving the corresponding line image in (a). (c) The same hyperspectral image as (b) but with the vertical axis converted to wavelength before (left) and after (right) deconvolution. (d) A spectrum cut at the green line in (c) before and after deconvolution.

shown in Supplementary Fig. 2(b,left). Due to the small tilt of the grating, the image is shifted in the y direction as a function of x, resulting in an angle between the transmission bands and the x axis. Since the hyperspectral image is a convolution of the laser beam shape and the emission spectrum which blurs the edges of the transmission bands, we sharpen the edges by deconvolving Supplementary Figure 2(a) out of Supplementary Figure 2(b). From the position of the four edges (red lines in Supplementary Figure 2(b), manually selected), a map from the y coordinates to the wavelength value was obtained. Supplementary Figure 2(b) can therefore be transformed to the hyperspectral image in Supplementary Figure 2(c). For Raman imaging, the tilt of the grating was adjusted to cover a slightly different spectral range. The new tilt value was obtained by matching the peak positions of the measured Raman spectra of PS and PMMA with the reference data.

2.2 Volumetric imaging

λ-OPM can capture volumetric hyperspectral data by scanning the position of either the sample or the laser beam. Two galvanometric mirrors (Galvo y and Galvo z), both placed conjugate to the pupil of O1, are used to control the position of the laser line. Galvo y scans the laser line in the y direction. When dithering back and forth in high speed, the laser line forms a light sheet and a whole plane in x-y can be imaged, as in a conventional OPM. Galvo z scans the laser line (or sheet) in z and de-scans the image while keeping tilt of the plane constant [3]. The sample is mounted on a motorized scanning stage (Thorlabs MLS203), which can be used to scan the sample in both x and y.

The field of view of the OPM is 500 μm × 400 μm. The maximum spectral range of a hyperspectral image is approximately 200 nm with the centre of the spectrum determined by the vertical location of the laser beam, i.e. scanning Galvo y changes the spectral range. In this work, we keep Galvo y fixed. The fluorescence measurements were performed with the laser line passing approximately through the centre of the field of view. For Raman scattering measurements, the laser was moved approximately 100 μm from the centre.

The theoretical detection NA of the OPM image is about 0.93, determined by O2 which has the smallest light cone of the 3 objectives. By imaging a sparse distribution of 200 nm diameter fluorescence beads (Tetraspeck microspheres, 0.2 μm blue/green/orange/dark red) in agarose gel, we found the actual resolution of the OPM to be approximately 650 nm × 650 nm × 3400 nm (FWHM) in the middle of the image; the resolution degrades towards the edge of the image due to stronger aberrations as shown in Supplementary Figure 3. When doing hyperspectral imaging, the resolution in the y direction is determined by the size of the laser beam, i.e. 8 to 24 μm (FWHM, from centre to edges). This also determines the spectral resolution to be between 13 and 40 nm. When imaging sparsely distributed objects that are smaller than the laser beam, the spectral resolution is not limited by the beam size but by the vertical size of the object. However, the position of the object relative to the laser beam can introduce a shift of the spectra. Deconvolving the object image improves both the spectral resolution and accuracy. In addition, as a general challenge for light sheet microscopy, scattering of the excitation light in the sample can reduce the contrast of the image as well as the spatial and spectral resolution. When necessary, the spectral resolution can be further enhanced by adding a slit on the remote image plane between O2 and O3, at a cost of photon loss.

3 System design

3.1 Water chamber fabrication

In any OPM design, O3 must be tilted with respect to O2, which creates obvious difficulties in capturing the rays propagating at high angles to the optical axis of O3. Traditionally this has been achieved with a high-NA-air-immersion objective (which cannot achieve the NA necessary to capture all the rays emitted by O2), a high-NA water immersion objective with a custom-made water chamber [2] or more recently a dedicated solid-immersion zero-working-distance OPM objective[4, 5]. Due to the cost and inflexibility of zero-working-distance lenses, we use a water chamber solution. An existing water-immersion objective (Nikon MRD77220, 20×, 1.1NA) was fitted with a custom-machined water chamber (see Supplementary Figure 4(A),(B)) which sat over the lens, and could be positioned accurately using a differential micrometer. O-ring seals ensured the water chamber did not leak, and the outermost optical surfaces consisted of glass coverslips cut to shape and glued onto the chamber housing. A separate mounting clamp held the water chamber tightly to the objective body. A translation stage attached between the clamp and the water chamber was used to adjust the position of O3 so that it focused on the outer surface of the coverslip to minimise spherical aberration.

3.2 Grating insert fabrication

λ-OPM is designed to rapidly and easily convert between a conventional OPM design and the hyperspectral imaging configuration. A custom insert for a commercial kinematic fluorescence filter cube (ThorLabs DFM1/M magnetic filter cube) was created by modifying of the existing DFM1T1 cube insert. One half of the insert was replacing with a custom-machined kinematic grating mount, and the existing half was milled to make room (see Supplementary Figure 4(C),(D)). The insert held a grating oriented such that the zero order reflection passes outside the system aperture. The first order diffraction propagates along the optical axis, through the tube lens and images onto the

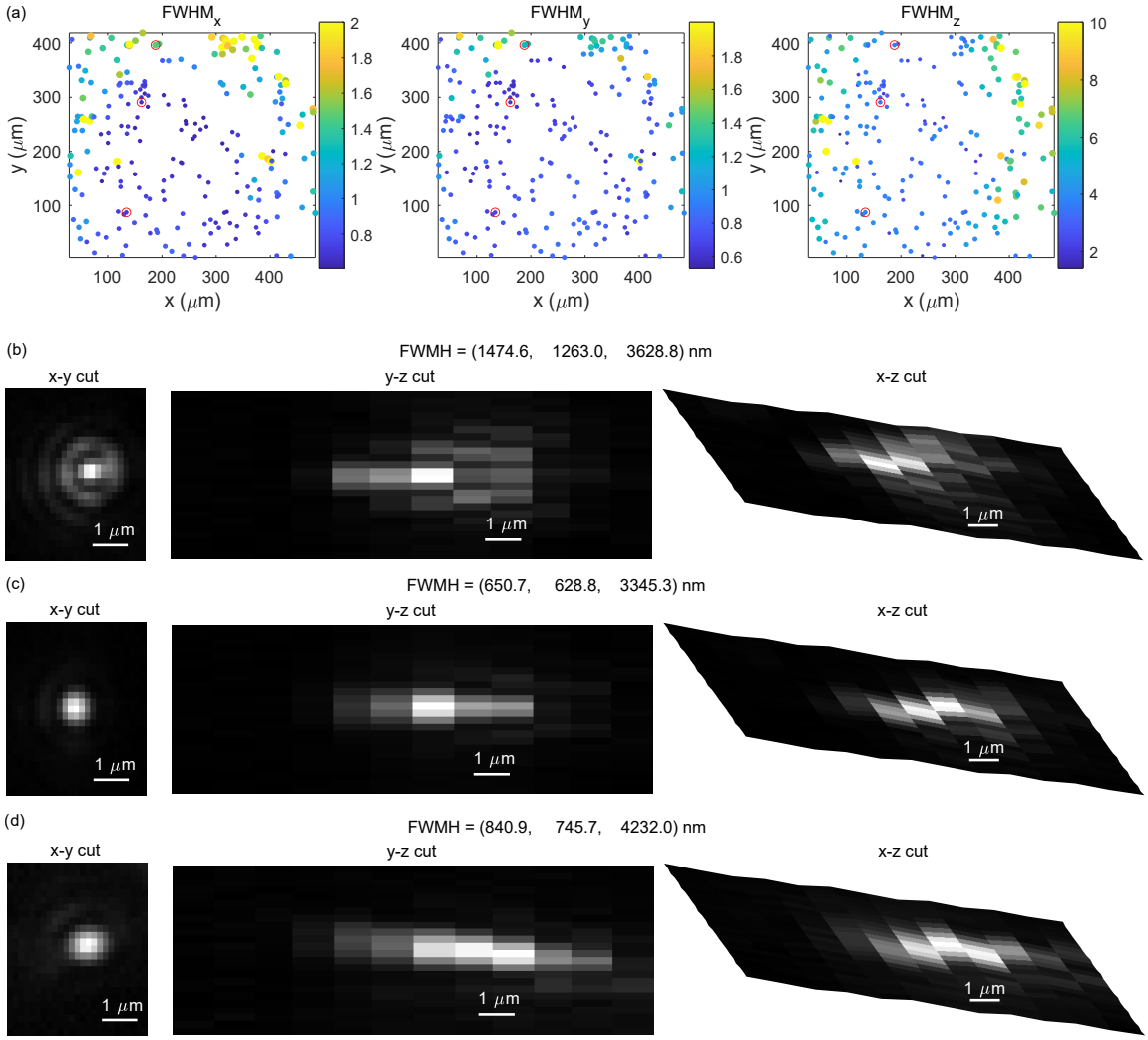

Supplementary Figure 3: (a) Distribution of the FWHM of the 3D PSF at different positions of the image. The resolution is evenly distributed in the middle 250 µm × 250 µm area and increases at the edges of the image. The values are obtained by fitting each the 3D images of 224 fluorescent beads with 3D Gaussian functions (least square method). (b-d) Sections in the middle of the images of the 3 beads marked by red circles in (a). The larger FWHM results from stronger aberrations near the edge of the field of view.

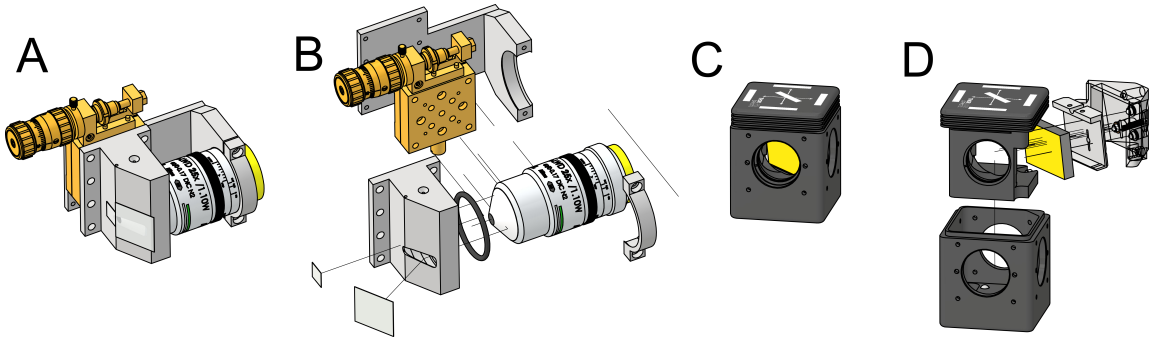

Supplementary Figure 4: Custom parts. (A) Assembled water chamber assembled onto a microscope objective. The focal position of the coverslip can be tuned using a differential micrometer. (B) Exploded diagram of (A). (C) Modified fluorescence filter cube containing a grating mounted in a custom kinematic mount. (D) Exploded version of (C), highlighting the custom-machined modified insert, grating mount, three-point kinematic adjusters and retaining spring.

camera. The three-point kinematic adjusters and retaining spring allow for small change of the grating tilt angle and therefore the spectral range detected by the camera.

A separate filter cube, containing a 532 nm dichroic mirror (Semrock DI03-R532-T1-25X36) and two band-pass filters (Semrock FF01-515/30-25 and FF01-582/64-25), could be used instead of the grating cube, allowing easy conversion between the hyperspectral imaging mode and conventional red and green filter channels.

3.3 Convolutional neural network for spectrum classification

The CNN used for classifying the Raman spectra contains one layer with filters = 64 and kernel size = 3. The training and test data were measured from 4 samples containing each of the 3 polymers (PS, PMMA, PA6) and pure agarose. Hyperspectral images were taken at different positions of both galvo mirrors and converted spectra with 20 cm^{-1} resolution and with binning of 10 pixels in the x direction. The Raman and fluorescence spectra of agarose and the confocal dish were obtained from the corresponding positions of the hyperspectral images measured from the pure agarose sample. The Raman spectra of PS, PMMA and PA6 were programmatically selected based on the the number of peaks in the spectra. In details, we smoothed each vertical line of the image (after rotation) with a Gaussian window and search for the peaks (MATLAB smoothdata and findpeaks) in two separate regimes, i.e. 700-1850 cm^{-1} and 2700-3200 cm^{-1}. When at least 3/4/3 (for PS/PMMA/PA6) peaks in the first regime and at least 2/1/1 (for PS/PMMA/PA6) peaks in the second regime were found, the corresponding spectrum was calculated (without smoothing) as training data.

The whole data set contains 14982 spectra (approximately 3000 for each class). The data were randomly shuffled and pre-processed, which included removing the linear trend (using scipy.signal.detrend) of the spectra, subtracting the mean, normalizing to the maximum and finally cropping to the range of 560 cm^{-1} to 3360 cm^{-1}. 80 % of the data were used for training and 20 % for testing. The final model converged after 200 epoches and reached an accuracy of over 98 % after 500 epoches, as shown in Supplementary Figure 5.

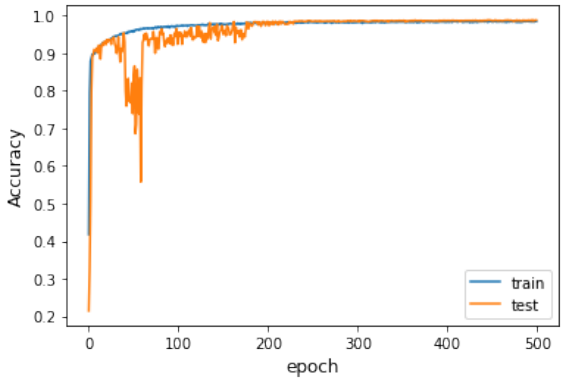

Supplementary Figure 5: Training and validation accuracy of the CNN model.

3.4 Component separation for Raman spectra of zebrafish embryo

From the measured Raman spectra of the zebrafish embryo, we extra the scattering intensity of 4 types of molecules, i.e. collagen, carotenoid, and lipids by simply calculating the size of the corresponding Raman peaks. For collagen, we calculated the average intensity of two peaks at 900-980 cm^{-1} and 1600-1680 cm^{-1}, and subtract the average of the nearby area at 980-1060 cm^{-1} and 1680-1760 cm^{-1}. For carotenoid, we calculated the average at 1100-1180 cm^{-1} and 1460-1580 cm^{-1} and subtract the average at 1300-1460 cm^{-1}. The lipids we calculated average difference between 2820-2900 cm^{-1} and 2740-2820 cm^{-1}. By subtracting the neighbouring area, the contribution of autofluoresence is largely suppressed.

References

[1] E. J. Botcherby, R. Juskaitis, M. J. Booth, and T. Wilson, "Aberration-free optical refocusing in high numerical aperture microscopy," *Opt. Lett., OL*, vol. 32, pp. 2007–2009, July 2007. Publisher: Optica Publishing Group.

[2] B. Yang, X. Chen, Y. Wang, S. Feng, V. Pessino, N. Stuurman, N. H. Cho, K. W. Cheng, S. J. Lord, L. Xu, D. Xie, R. D. Mullins, M. D. Leonetti, and B. Huang, "Epi-illumination SPIM for volumetric imaging with high spatial-temporal resolution," *Nat Methods*, vol. 16, pp. 501–504, June 2019. Bandiera_abtest: a Cg_type: Nature Research Journals Number: 6 Primary_atype: Research Publisher: Nature Publishing Group Subject_term: High-throughput screening;Light-sheet microscopy;Super-resolution microscopy Subject_term_id: high-throughput-screening;light-sheet-microscopy;super-resolution-microscopy.

[3] M. Kumar, S. Kishore, J. Nasenbeny, D. L. McLean, and Y. Kozorovitskiy, "Integrated one- and two-photon scanned oblique plane illumination (SOPi) microscopy for rapid volumetric imaging," *Opt. Express, OE*, vol. 26, pp. 13027–13041, May 2018. Publisher: Optical Society of America.

[4] E. Sapoznik, B.-J. Chang, J. Huh, R. J. Ju, E. V. Azarova, T. Pohlkamp, E. S. Welf, D. Broadbent, A. F. Carisey, S. J. Stehbens, K.-M. Lee, A. Marín, A. B. Hanker, J. C. Schmidt, C. L.

Arteaga, B. Yang, Y. Kobayashi, P. R. Tata, R. Kruithoff, K. Doubrovinski, D. P. Shepherd, A. Millett-Sikking, A. G. York, K. M. Dean, and R. P. Fiolka, "A versatile oblique plane microscope for large-scale and high-resolution imaging of subcellular dynamics," *eLife*, vol. 9, p. e57681, Nov. 2020. Publisher: eLife Sciences Publications, Ltd.

[5] B. Yang, M. Lange, A. Millett-Sikking, X. Zhao, J. Bragantini, S. VijayKumar, M. Kamb, R. Gomez-Sjoberg, A. C. Solak, W. Wang, H. Kobayashi, M. N. McCarroll, L. W. Whitehead, R. P. Fiolka, T. B. Kornberg, A. G. York, and L. A. Royer, "Daxi-high-resolution, large imaging volume and multi-view single-objective light-sheet microscopy," *NATURE METHODS*, 2022.